Korean J. Chem. Eng., 33(11), 3194-3202 (2016)
DOI: 10.1007/s11814-016-0166-7

pISSN: 0256-1115
eISSN: 1975-7220

Modeling of gas permeation through mixed matrix membranes using a comprehensive computational method

Majid Pakizeh†, Salman Ofoghi, and Seyed Heydar Rajaee Shooshtari

Department of Chemical Engineering, Faculty of Engineering, Ferdowsi University of Mashhad,
P. O. Box 9177948974, Mashhad, Iran
(*Received 3 January 2016 • accepted 15 June 2016*)

Abstract−Three different morphologies can occur at the interface of inorganic and polymeric phases in mixed matrix membranes (MMMs). These morphologies are characterized by their different parameters such as partial pore blockage factor (α), polymer chain rigidification factor (β), and thickness of rigidified layer or void region. In this study, the morphology of three MMMs has been evaluated using a comprehensive computational method. The average absolute relative error (%AARE) is used as a criterion for optimizing three various MMM morphological parameters. According to the obtained optimum parameters, it was confirmed that two MMMs of C60/Matrimid and PVAc-Zeolite 4A have pore blockage and polymer chain rigidified defects. The results show that the morphology of ZIF-8/6FDA-DAM can be considered as an ideal morphology. After obtaining the morphological parameters, the permeability of the studied MMMs was predicted based on the modified Maxwell model and good agreement was observed between the calculated value and the experimental data.

Keywords: Mixed Matrix Membranes, Gas Permeability Prediction, Morphological Parameters, Optimization

INTRODUCTION

Thomas Graham introduced the application of membrane technology in gas separation for the first time [1]. Polymers are more commonly employed for membrane preparation because of their low cost, high processing capability and appropriate intrinsic permeation properties. On the other hand, inorganic materials possess a high capability to separate gas species even in severe environments and under higher temperature and pressure conditions. However, their applications are still limited because of the high cost, the problems in flexibility and reproducibility in the preparation step as well as hard production of spiral wound or hollow fiber modules [2-4]. Mixed matrix membranes (MMMs) are novel membranes that are combinations of inorganic fillers dispersed in a polymer matrix [5]. In fact, an MMM contains the economic advantages of polymers and also high selectivity of the dispersed fillers and desirable mechanical properties. These new materials may have effective applications in known gas separation processes, separation of oxygen-nitrogen mixture and dehydration or sweetening of raw natural gases. Porous molecular-sieve type materials, including zeolites [6,7], carbon molecular sieves (CMSs) [8,9], silica [10], and metal organic frameworks (MOF) [11], have commonly been used as inorganic fillers in MMMs. Since the molecular-sieve type fillers used in MMMs are capable of separating different molecules based on their size and shape, both permeability and selectivity can be improved compared to the polymeric membranes. For example, Zeolite NaA is very effective as a molecular-sieve filler in the separation of oxygen-nitrogen mixtures [7]. Ideal permeation models for MMMs including porous fillers are used to estimate the effective permeability of a gaseous penetrant through these membranes. These models are only functions of continuous polymeric phase permeability, dispersed phase permeability and volume fraction of dispersed phase. Bouma et al. applied the Maxwell-Wagner-Sillar (MWS) model to predict the effective permeability of a MMM with a dilute dispersion of ellipsoids [9,12,13].

$$P_{eff}=P_c\frac{nP_d+(1-n)P_c-(1-n)\phi_d(P_c-P_d)}{nP_d+(1-n)P_c+n\phi_d(P_c-P_d)} \tag{1}$$

where P_{eff} is the effective permeability of MMM, P_c is the permeability of pure polymer, P_d is the permeability of the filler, ϕ_d is the volume fraction of the filler in MMM and n is the particle shape factor. For n=0, this expression is simplified to a parallel two-layer model that can be expressed as an arithmetic mean of the inorganic and polymeric phase permeabilities [9,14]:

$$P_{eff}=P_c(1-\phi_d)+\phi_d P_d \tag{2}$$

Moreover, when n=1.0 the MWS model is converted to the series two-layer model [9,14]:

$$\frac{1}{P_{eff}}=\frac{1-\phi_d}{P_c}+\frac{\phi_d}{P_d} \tag{3}$$

If n=1/3, the MWS model changes to the following equation known as Maxwell's model:

$$P_{eff}=P_c\frac{P_d+2P_c-2\phi_d(P_c-P_d)}{P_d+2P_c+\phi_d(P_c-P_d)} \tag{4}$$

Eq. (4) was initially developed to predict electrical conduction through composite materials [15]. The Maxwell equation is appli-

†To whom correspondence should be addressed.
E-mail: pakizeh@um.ac.ir

cable to a dilute suspension of spheres and can only be applicable for low loading where the volume fraction of filler particles is less than about 20% [9,13,14,16]. This assumption of low loading is essential because the streamlines around particles should not be affected by the presence of nearby particles. In addition, the Maxwell model cannot predict the permeability of MMMs at the maximum packing volume fraction of the filler particles. Also, the Maxwell model does not take into account particle size distribution, particle shape, and aggregation of particles [13]. To calculate the permeability of an MMM with a high filler loading, the Bruggeman model, which was originally developed for the dielectric constant of particulate composites, can be used [17]. This model takes into account the effect of higher loading of the filler and the random distribution of spherical particles, which leads to the following [9]:

$$\left(\frac{(p_{eff}/p_c)-(p_d/p_c)}{1-(p_d/p_c)}\right)\left(\frac{p_{eff}}{p_c}\right)^{-1/3}=1-\phi_d \tag{5}$$

Although the results of the Bruggeman model are acceptable at high loadings, this model cannot predict the permeability of the MMMs at the maximum loading of filler particles just similar to the Maxwell model. Furthermore, it does not consider the particle size distribution, the particle shape, and the aggregation of particles. To estimate the effective permeability by using this equation requires a trial and error procedure [13]. The Lewis-Nielsen model [18,19], which was initially proposed for the elastic modulus of particulate composites, can be used to predict permeability [13]:

$$p_{eff}=p_c\left(\frac{1+2(((p_d/p_c)-1)/((p_d/p_c)+2))\phi_d}{1-(((p_d/p_c)-1)/((p_d/p_c)+2))\phi_d\psi}\right) \tag{6}$$

where

$$\psi=1+\left(\frac{1-\phi_m}{\phi_m^2}\right)\phi_d \tag{7}$$

Here ϕ_m is the maximum packing volume fraction of the filler, which is 0.64 for random close packing of uniform spheres. The effects of morphology on permeability are considered in this model because ϕ_m is a function of particle size distribution, particle shape, and aggregation of particles. If interfacial defects between continuous and dispersed phases are neglected, all of the above-mentioned models are applicable for predicting the permeation through the MMM. Mostly, the fabrication of an MMM with no interfacial defects is very difficult. These defects affect membrane performance and should be considered in predictive models. These interface defects occur due to the different intrinsic properties of the polymer and inorganic phases [20]. Generally, the four types of morphology that can occur at the interface of MMMs are ideal contact, rigidified layer, total or partial pore blockage of filler and void formation [5]. Fig. 1 shows a schematic diagram of various probable MMM morphologies [21]. Case I shows an ideal contact between the filler and polymer interface. Ideal predictive models that are mentioned above can be used to predict the gas permeability through this type of MMM. However, case II demonstrates pore blockage defect at the interface of the filler and polymer. In this case an interface is observed in which the surface pores of the filler have been partially plugged by polymer chains [5,22]. In the rigidified layer

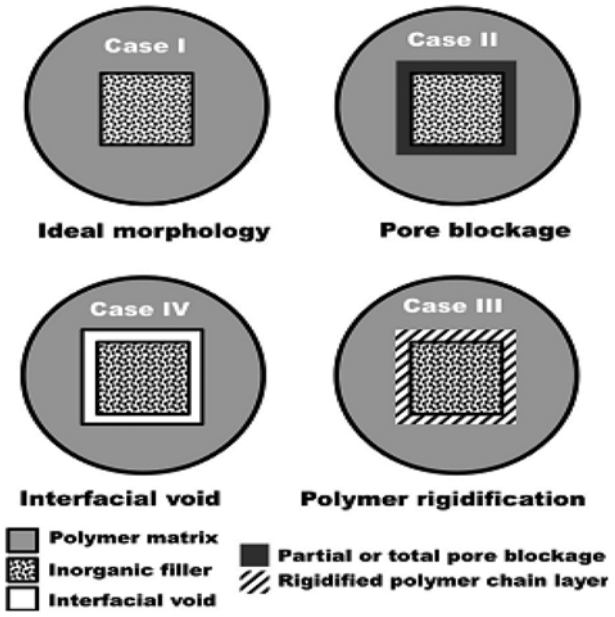

Fig. 1. Schematic diagram of various non ideal MMM morphologies: (case I) ideal contact, (case II) pore blockage, (case III) rigidified polymer chain layer, (case IV) interfacial voids [18].

(case III), the mobility of polymer chains is reduced compared to the bulk of the polymer and this rigidified polymer layer around the filler shows a lower permeability and higher selectivity than the bulk polymer [20]. Sometimes the separation of polymer chains from the filler surface causes void formation (case IV). Poor polymer-particle interaction as well as the repulsive force between the polymer and filler are the other reasons for the formation of interface voids [20].

Mahajan and Koros [7] investigated the effect of interface defect layer on the permeability of penetrants in the MMMs. The permeability of penetrants in the MMMs which contain filler phase, polymer phase and interface layer may be modeled by using a two-step method. In the first step, the Maxwell equation (Eq. (4)) can be used to obtain the permeability of the combined interface rigidified layer and the filler in which the rigidified layer is the continuous phase and the filler is the dispersed phase. Thus, the permeability of the combined interface layer and filler phase is obtained as follows:

$$p_{eff}=p_I\frac{p_d+2p_I-2\phi_s(p_I-p_d)}{p_d+2p_I+\phi_s(p_I-p_d)} \tag{8}$$

where P_{eff} is the permeability of the combined filler and interface layer phases, P_d is the permeability of the disperse phase, P_I is the permeability of the interface layer and ϕ_s is the volume fraction of the disperse phase in the combined filler and interface layer phase. ϕ_s can be calculated by using the following equation:

$$\phi_s=\frac{\phi_d}{\phi_d+\phi_i}=\frac{r_d^3}{(r_d+I_i)^3} \tag{9}$$

where ϕ_i is the volume fraction of the interface layer, r_d is mean radius of the dispersed filler and I_i is the interface layer thickness. At the second step, this calculated P_{eff} can be used with the contin-

uous polymer phase permeability P_c to obtain a predicted permeability of P_{MMM}, using the following equation:

$$P_{MMM}=P_c\frac{P_{eff}+2P_c-2(\phi_d+\phi_I)(P_c-P_{eff})}{P_{eff}+2P_c+(\phi_d+\phi_I)(P_I-P_{eff})} \quad (10)$$

Hashemifard et al. [23] defined the average absolute relative error percent (%AARE) and standard deviation (σ) to compare the predictive models. The results showed that %AARE decreases in the following order for the various models: Lewis-Nielsen model> Maxwell model>modified Lewis-Nielsen model>modified Maxwell model>Felske model. The average absolute relative error percent (%AARE) and the standard deviation (σ) are defined as follows:

$$\%AARE=\frac{100}{NDP}\sum_{i=1}^{NDP}\left|\frac{P_i^{cal}-P_i^{exp}}{P_i^{exp}}\right| \quad (11)$$

$$\sigma=\sqrt{\frac{1}{NDP}\sum_{i=1}^{NDP}(\%RE-\%ARE)^2} \quad (12)$$

where NDP is the number of data points and P_i^{cal} and P_i^{exp} are the calculated and experimental permeabilities, respectively. The percentage of relative errors ($\%RE_i$) and the percentage of absolute relative errors (%ARE) are given by:

$$\%RE_i=\frac{P_i^{cal}-P_i^{exp}}{P_i^{exp}} \quad (13)$$

$$\%ARE=\frac{100}{NDP}\sum_{i=1}^{NDP}\%RE \quad (14)$$

Gheimasi et al. [24] considered the effect of pore blockage and polymer chain rigidified in the prediction model and defined P'_d and P'_c as follows:

$$P'_d=(1-\alpha)*P_d \quad (15)$$

$$P'_c=\frac{P_c}{\beta} \quad (16)$$

In these equations α and β are the pore blockage factor and the polymer chain rigidification factor, respectively. These adjustable parameters are obtained through an optimization procedure. By this definition, the effect of pore blockage and polymer chain rigidified in modified Maxwell model is considered and the permeability of the MMM is predicted by the following equations:

$$P_{ps}=P_c\frac{P'_d+2P'_c-2\phi_s(P'_c-P'_d)}{P'_d+2P'_c+\phi_s(P'_c-P'_d)} \quad (17)$$

$$P_r=\frac{P_M}{P_c}=\frac{P_{ps}+2P_c-2(\phi_d+\phi_I)(P_c-P_{ps})}{P_{ps}+2P_c+(\phi_d+\phi_I)(P_I-P_{ps})} \quad (18)$$

Here P_{ps} is the permeability of pseudo-disperse phase, and ϕ_s and ϕ_I are calculated from Eq. (9). In Gheimasi et al. model, the permeability of the filler and the thickness of the interface layer were considered to be known parameters that must be obtained experimentally. The Maxwell-Stefan formulation for predicting the diffusive transport in MMMs with oriented selective flakes has also been reported in [25,26]. Singh et al. developed methods for the automated construction of detailed and large-scale 3D MMM models and solved them by the finite element method [27]. Yang and colleagues presented the first numerical method for the prediction of effective diffusivity in hollow fiber MMMs [28]. Recently, Vinh-Thang and Kaliaguine [21] presented a new comprehensive computational strategy for fitting experimental permeation data on the permeation model. Note that in almost all reported MMM permeation models, the permeability of the filler has been considered as a known parameter, while in this model it is considered as an adjustable parameter which should be extracted from fitting data. However, to the best of our knowledge, there are no published studies about morphology prediction of an MMM using its experimental permeation data. We used the Vinh-Thang and Kaliaguine strategy to recognize different morphologies of the MMMs. Here, a genetic algorithm program was developed to minimize %AARE as an object function, and the values of the parameters of the genetic algorithm code are given in Table 1.

Table 1. Best values of the computational parameters used

Parameters	Value
Maximum number of generations	10000
Total number of chromosomes in the population	50
Accuracy	0.0001
Crossover probability	0.25
Mutation probability	0.01

COMPUTATIONAL STRATEGY

For fitting experimental permeation data of the MMMs, Vinh-Thang and Kaliaguine strategy was used in this study. In this approach, partial pore blockage, polymer chain rigidification and void defects are simultaneously taken into account. According to this method, the term ϕ_d/P_d can be used as a critical indication for morphology type of the MMMs when applying Eq. (3). A negative value for this term is an indicator of void defect morphology type. Otherwise, pore blockage or polymer chain rigidification defects could probably occur. In the case of pore blockage and polymer chain rigidification morphologies, this method has four steps to estimate the MMMs morphological parameters. In the final step, one of the known MMM models is used to predict gas permeation through the MMMs and optimize the gas permeability of the fillers (P_d). The adjustable parameters (α, β, P_d and I_{op}) should be optimized by minimizing %AARE. In all steps, the filler loading (ϕ_d) is considered as a variable parameter. In step I, just the effect of partial pore blockage is considered, whereas polymer chain rigidification is temporarily neglected. In this step, two adjustable parameters that consist of the pore blockage factor (α) and filler permeability (P_d) are obtained.

Fig. 2 shows a flowchart of optimization method in step I. As shown, $P_{d\,min}$, $\alpha_{p\,max}$ and $P_{d\,max}$, $\alpha_{s\,max}$ are determined using parallel and series models, respectively. These derived parameters are used in the next steps. In step II, only polymer chain rigidification defect is considered and pore blockage defect is neglected. Both $P_{d\,max}$ and $P_{d\,min}$ parameters estimated in step I are replaced by P_d in the series and parallel models. Chain mobility factor (β) and interface layer thickness (I_{op}) as two adjusted parameters are determined in this step. Fig. 3 shows a determination flowchart diagram for the

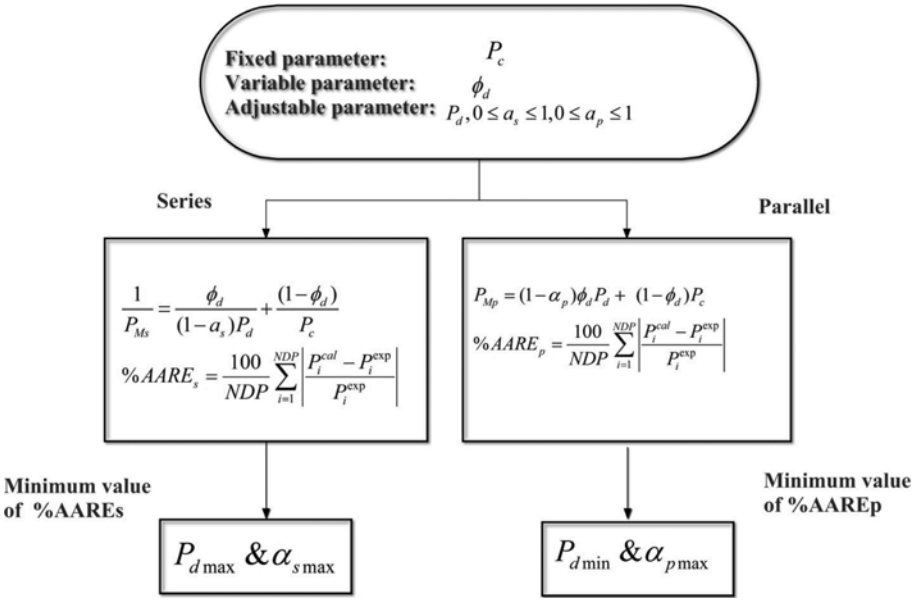

Fig. 2. Step I: Calculation routs of $P_{d\,min}$, $\alpha_{p\,max}$, and $P_{d\,max}$, $\alpha_{s\,max}$ [18].

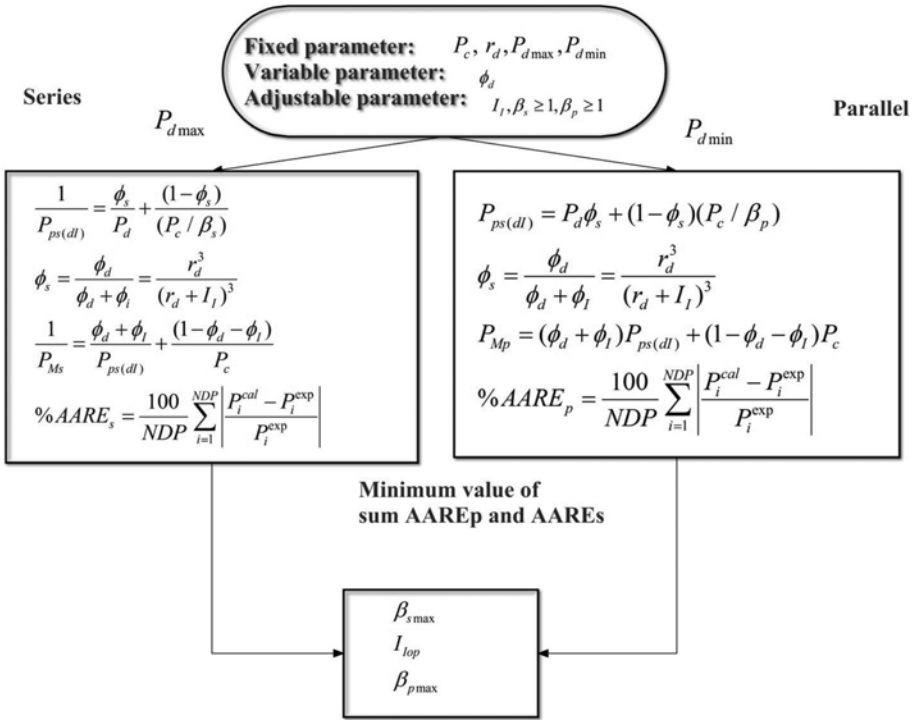

Fig. 3. Step II: Determination of $\beta_{s\,max}$, $\beta_{p\,max}$ and I_{op} [18].

parameters βs_{max}, $\beta_{p\,max}$ and I_{op}.

In step III, the two defects, pore blockage and rigidified layer, are simultaneously considered in both the series and the parallel two-layer models. The interface thickness that was optimized in step II is used in this step as a parameter. The minimized values of %AAREs and %AAREp are used as the criteria to obtain the optimized α_{sop}, α_{pop}, β_{sop} and β_{pop} parameters. As shown in Fig. 4, the overall optimized α_{op} and β_{op} are arithmetic means. From step I to III, three morphological parameters (α_{op}, β_{op} and I_{op}) can be mathematically derived using the above series and parallel models with minimum error. In the last step, an overall MMM model should be applied to predict the overall permeation through the MMMs at different filler loadings. To consider the interfacial defects, the corrected expressions P_d^* and P_c^* are used instead of P_d and P_c. Fig. 5 shows a determination flowchart of the optimized P_{dop}.

For determination of optimized interface void thickness and per-

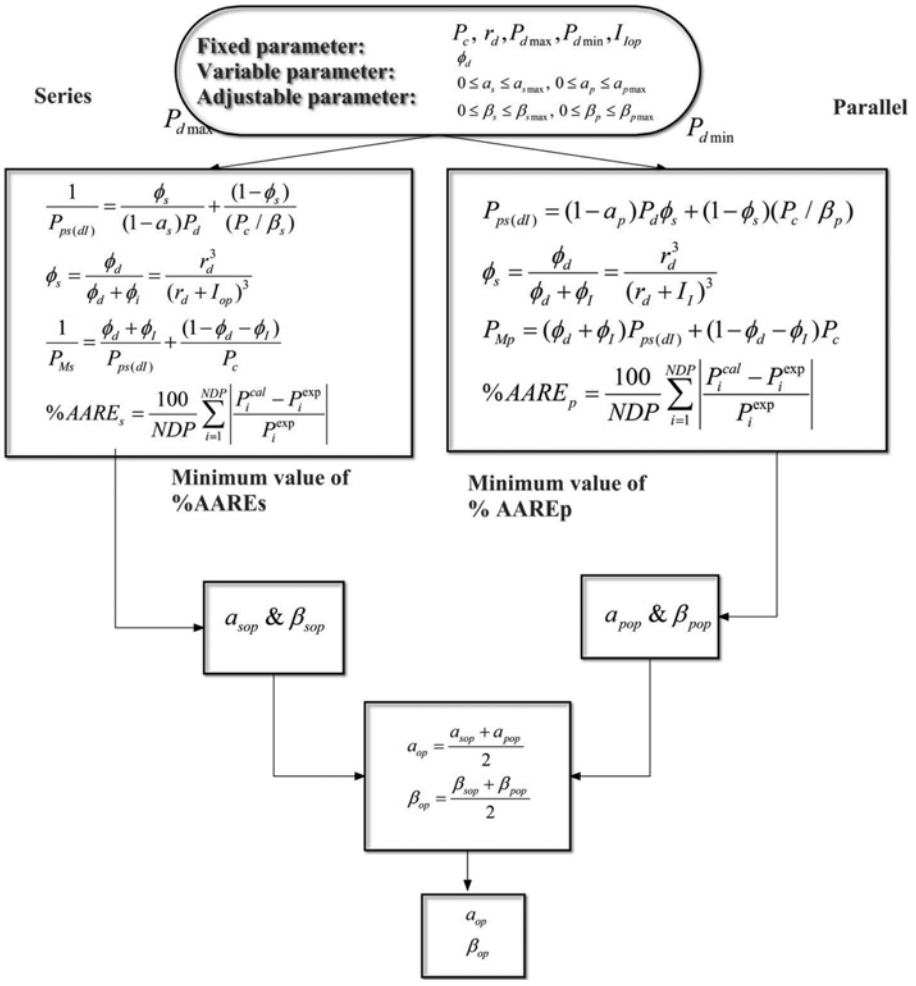

Fig. 4. Step III: Determination α_{op}, β_{op} [18].

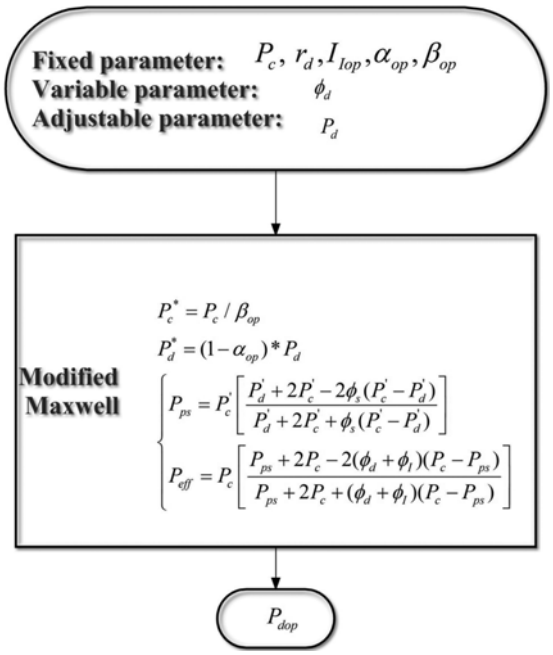

Fig. 5. Step IV: Determination of P_{dop} [18].

meability of this region, two optimization steps were used in this study. Actually, the gas diffusion through the void region may be greater than the small pore of the filler particles. Then, the gas diffusion through the inorganic fillers and rigidified polymer chain layer can be neglected compared to the void region (P_d=0, α=0, β=1). For this morphology, the thickness of the void region and the permeability of the penetrants in this region should be optimized. Thus, the Vinh-Thang procedure was used here for estimation of these parameters. In the first step, the interface thickness of the void region and the maximum and the minimum of penetrants' permeability in this zone were determined (Fig. 6). In the last step, the exact value of permeability of penetrants in the void region (P_{vop}) was determined, as shown in Fig. 7, and then the modified Maxwell model was used to predict the gas permeability through the MMMs (P_{eff}).

RESULTS AND DISCUSSION

To predict the morphology of the studied MMMs, the experimental gas permeation data through three MMMs that are published in the literature were used. Tables 2-4 show the experimental permeation data for three different types of MMMs. Table 2 is

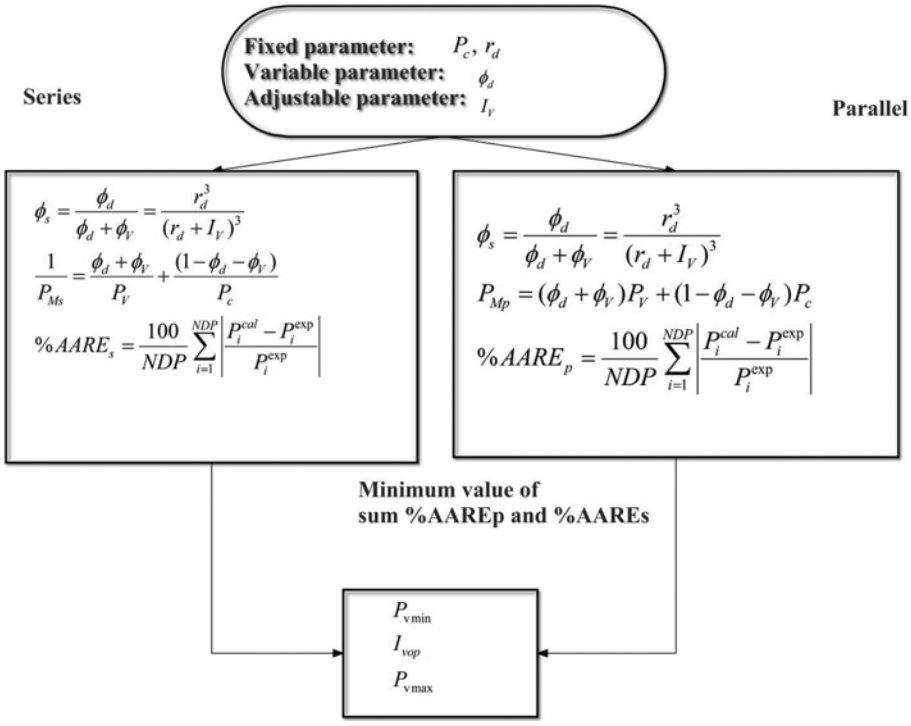

Fig. 6. Step I: Determination of P_{vmax}, I_{vop} and P_{Vmin} [18].

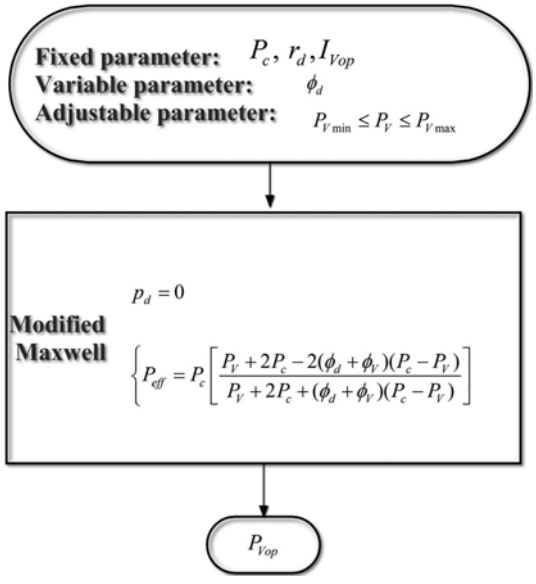

Fig. 7. Step II: Determination of P_{Vop} [18].

related to the experimental permeability of He and N_2 through C60/Matrimid MMM [29], while Table 3 shows the experimental permeability of C_3H_6 and C_3H_8 through ZIF-8/6FDA-DAM MMM [30] and the experimental O_2 permeability and O_2/N_2 selectivity of Zeolite 4A/PVAc MMM are presented in Table 4 [31].

1. C60/Matrimid MMM (Set 1)

In set 1, the permeation data that were reported for the separation of He and N_2 mixtures volume fraction of C60 filler are low (see Table 2). The C60 particle diameter is assumed to be 1 nm.

Table 2. Experimental permeability of He and N_2 in C60/MMM (set 1)

ϕ_d (vol%)	Permeability (Barrer)		Ref.
	He	N_2	
0	25	0.275	[25]
1.87	21	0.229	
3.76	18	0.184	
7.62	17	0.161	

Table 3. Experimental permeability of C_3H_6 and C_3H_8 in ZIF-8/6FDA-DAM MMM (set 2)

ϕ_d (wt%)	ϕ_d (vol%)	$P_{C_3H_6}$ (Barrer)	$P_{C_3H_8}$ (Barrer)	Ref.
0	0	15.7±1.1	1.27±0.05	[26]
16.4	23.8	27.6±1.6	1.47±0.13	
28.7	39.0	39.8±0.2	1.63±0.01	
48.0	59.5	56.2±1.9	1.81±0.08	

Table 4. Experimental permeability O_2 and selectivity O_2/N_2 of Zeolite4A/PVAc MMM (set 3)

ϕ_d (vol%)	P_{O_2} (Barrer)	α_{O_2/N_2}	Ref.
0	0.5	5.9	[27]
15	0.45	7.3-7.6	
25	0.4	8.3-8.5	
40	0.28-0.35	9.7-10.4	

Therefore, the radius of C60 particle is equal to 0.5 nanometers [32]. By evaluating the term ϕ_d/p_d for this data set from the series

Table 5. Calculated ϕ_d/p_d parameter for C60/Matrimid MMM

ϕ_d (vol%)	P_{He}	ϕ_d/p_d
0	25	0
1.87	21	0.00837
3.76	18	0.01706
7.62	17	0.02187

Table 6. Morphological parameters for three different MMMs

MMM type	α_{op}	β_{op}	I_{op} (nm)	P_{dop} (Barrer)
C60/Matrimid (set1)	0.934	3.630	0.361	224.93
ZIF-8/6FDA-DAM (set 2)	0.035	1.520	14.398	893.961
Zeolite 4A/PVAc (set 2)	0.325	1.715	372.978	0.459

model (Eq. (3)), we can estimate the morphology of the interface of the C60 filler and Matrimid polymer. The calculated ϕ_d/p_d parameter for C60/Matrimid MMM in different filler loadings is presented in Table 5. The positive values of ϕ_d/p_d indicate that voids are not formed in each filler loading. For this reason, we applied only pore blockage and rigidified optimization procedures to predict the morphology of C60/Matrimid MMM (Steps I to IV). Considering the He and N_2 permeation data (Table 2), one can see that by increasing C60 as the filler particle in polymer matrix, the permeability of two gases is decreased. This observation indicates that C60/Matrimid MMM has rigidified polymer or pore blockage and both morphologies simultaneously.

Note that in the Vinh-Thang procedure, the permeability data of a smaller penetrant is used to optimize the morphological parameters. He and N_2 have 2.6 Å and 3.64 Å kinetic diameters, respectively. Therefore, the permeability data for He (as small gas) were used to obtain the morphological parameters. The estimated morphological parameters for C60/Matrimid MMMs are depicted in Table 6. As can be seen, pore blockage parameter factor (α_{op}) for this MMM has a high value (0.934), indicating that the pores of the C60 molecule are mostly blocked by polymer chains and appear to serve as impenetrable particles within the polymer matrix.

Also, a high value was determined for the chain rigidified factor β_{op} (3.63). Considering $P_c^*=P_c/\beta$, a higher value of β (greater than unity) is an indicator of rigidified polymer case. Thus, by considering both high values of α_{op} and β_{op}, we concluded that both rigidified and pore blockage morphologies occurred simultaneously for this MMM. This result is confirmed by the experimental study of Chung et al. [29], who reported that by incorporating C60 as the filler particle, the glass transition temperature of polymer had increased. This reveals that the chain polymer rigidified defect has occurred in C60/Matrimid MMM and the high value of the calculated β_{op} is reasonable. In the last step the modified Maxwell model is applied to predict the overall permeation properties of C60/ Matrimid MMMs at different filler loadings. Table 7 and Fig. 8 exhibit the modified Maxwell model permeability of He prediction in C60/Matrimid MMM at different filler loadings. As expected, an excellent agreement can be observed in Fig. 8 between model prediction and experimental data for C60/Matrimid MMM. Also, the ideal Maxwell model predictions are shown in this Figure. The value of %AARE (6.1) in Table 7 indicates that the prediction procedure is valid.

Table 7. Comparison of experimental data and model prediction of He permeability through C60/Matrimid MMM

ϕ_d (vol%)	Experimental data	Model prediction	%AARE
0	25	25	
1.87	21	22.9	
3.76	18	20.8	
7.62	17	17	
			6.1

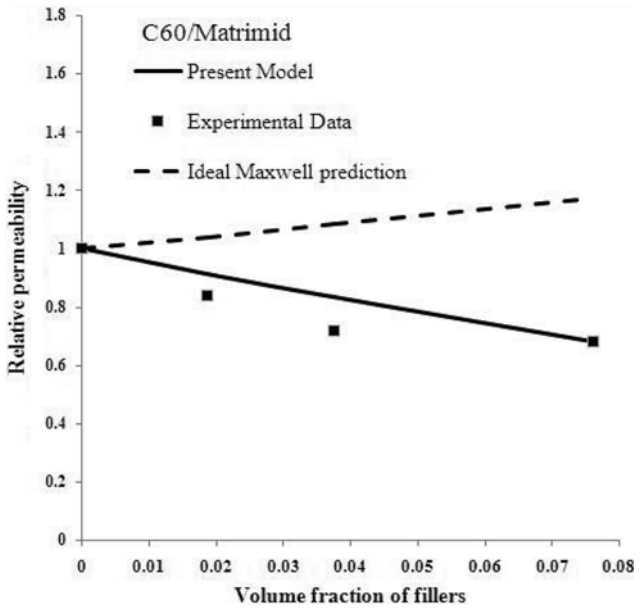

Fig. 8. Comparison between present model and ideal Maxwell model predictions with experimental relative permeability (set 1).

2. ZIF-8/6FDA-DAM MMM (Set 2)

For separation of C_3H_6 and C_3H_8 mixtures, Zhang et al. [30] fabricated a new MMM that consisted of 6FDA-DAM polyimide and a zeolitic imidazolate framework (ZIF-8). ZIF-8 ($Zn(MeIM)_2$, MeIM=2-methylimidazole) is the most popular in ZIFs and its particle diameter is about 200 nm [30]. The permeability data of C_3H_6 gas (as a smaller penetrant) should be used to optimize the morphological parameters when Vinh-Thang procedure is applied. The calculated ϕ_d/p_d parameter depicted in Table 8 shows that the interface of ZIF-8 filler and 6FDA-DAM as polymer is void.

Void thickness (I_{vop}) for this MMM was estimated to be about 7.195 nm according to the mentioned procedure. This low value of void thickness parameter implies that void morphology in the

Table 8. Calculated ϕ_d/p_d parameter for ZIF-8/ 6FDA-DAM MMM

ϕ_d (vol%)	$P_{C_3H_6}$	ϕ_d/p_d
0	15.7	0
23.8	27.6	−0.012
39.0	39.8	−0.014
59.5	56.2	−0.008

MMM happened in a low content. Moreover, the amount of ϕ_d/p_d is very close to the critical value (zero), and thus it is not unrealistic to neglect this defect. This result is consistent with SEM images and gas separation performance of the mentioned MMM. The relatively low negative value of ϕ_d/p_d is due to the existence of a few non-ideal clusters of ZIF-8 with size ranging from 500 nm to several microns that was also reported in the experimental study reported in [30]. After this, pore blockage and polymer chain rigidification morphologies were also examined for this MMM, and finally the optimized morphology parameters for each case were estimated and summarized in Table 6.

The optimized pore blockage factor (α) equals 0.035, indicating that polymer chains did not penetrate into the pore aperture of ZIF-8 filler and pores of the filler were not blocked. The low values of calculated rigidified factor (β=1.52) and rigidified layer thickness (I=14.398 nm) revealed that a rigidified polymer chain for this MMM occurred at a very low content. Therefore, it may be concluded that pore blockage and rigidified polymer chain defects have not occurred for this MMM. Considering the obtained results here and the interesting experimental data that exceed the Robeson trade-off bound, nearly ideal morphology can be considered for this MMM. To predict the permeability of the MMM and the permeability of the optimized filler, we used the last step of the procedure (see Table 9 and Fig. 9). In Fig. 9, the prediction of relative permeability of C_3H_6 and the prediction of the ideal Maxwell model versus volume fraction of fillers are plotted. A good agreement between the predicted permeability and experimental permeability is visible. The low amount of AARE% (3.3) confirms this proper fitting between the predicted values and experimental data.

Table 9. Comparison of experimental data and model prediction of C_3H_6 permeability through ZIF-8/ 6FDA-DAM MMM

ϕ_d (vol%)	Experimental data	Model prediction	%AARE
0	15.7	15.7	
23.8	27.6	26.4	
39.0	39.8	36.2	
59.5	56.2	56.2	
			3.3

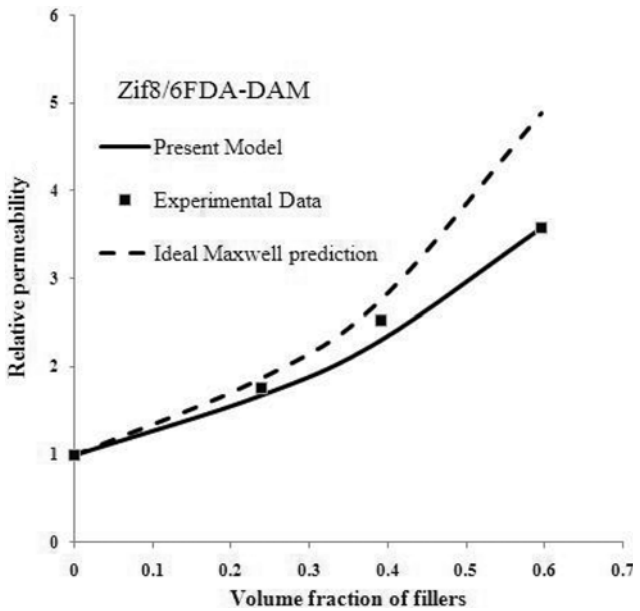

Fig. 9. Comparison between present model and ideal Maxwell model predictions with experimental relative permeability (set 2).

3. Zeolite 4A/PVAc MMM (Set 3)

For the O_2/N_2 separation, Mahajan and Koros [31] fabricated the Zeolite4A/PVAc MMM in which the average particle size of Zeolite 4A was reported to be in the range of 0.5-1.5 μm [33]. They claimed that a good adhesion between the filler and polymer occurs and a rigidified layer is formed around Zeolite 4A. Zeolite 4A is an attractive filler for O_2/N_2 separations because it possesses an eight-sided aperture with an effective aperture size of 3.8 Å that falls between the sizes of these molecules [20]. O_2 is a smaller molecule since gas kinetic diameters of O_2 and N_2 are 3.46 Å, 3.64 Å, respectively [29]. Pore blockage and rigidified optimization procedures should be applied to predict the morphology of Zeolite4A/PVAc MMM since for each filler loading the value of ϕ_d/p_d has a positive value (Table 10). The morphological parameters for this MMM were previously presented in Table 6.

In this table, the I_{op} and β parameters were calculated as 372.978 nm and 1.715, respectively, indicating that rigidified layer morphology has occurred. The experimental data also confirm this finding, because the permeability of both gases was decreased by filler loading, while the selectivity of O_2/N_2 increased. In another study, Mahajan et al. derived the parameters to be β=4.2 and I_{op}= 640 nm by simple fitting of experimental data on the modified Maxwell. Though, they did not consider a pore blockage defect, and also P_d was assumed to be a known parameter (i.e., 0.77 Barrer) [14], while P_d should be optimized because the permeation property of fillers in pure-filler thin membrane is likely to be different from that in the MMM. For this set of data, the optimized O_2 Zeolite permeability (P_d=0.549 Barrer) is significantly smaller than that reported by Mahjan et al. To predict the permeability of O_2 in this MMM, the last step optimization procedure was used

Table 10. Calculated ϕ_d/p_d parameter for Zeolite 4A/ PVAc MMM

ϕ_d (vol%)	P_{O_2}	ϕ_d/p_d
0	0.5	0.00
15	0.45	0.52
25	0.4	1.00
40	0.315 (0.28-0.35)	1.97

Table 11. Comparison of experimental data and model prediction of O_2 permeability through Zeolite 4A/PVAc MMM

ϕ_d (vol%)	Experimental data	Model prediction	%AARE
0	0.5	0.5	
15	0.45	0.43	
25	0.4	0.39	
40	0.315	0.315	
			2.2

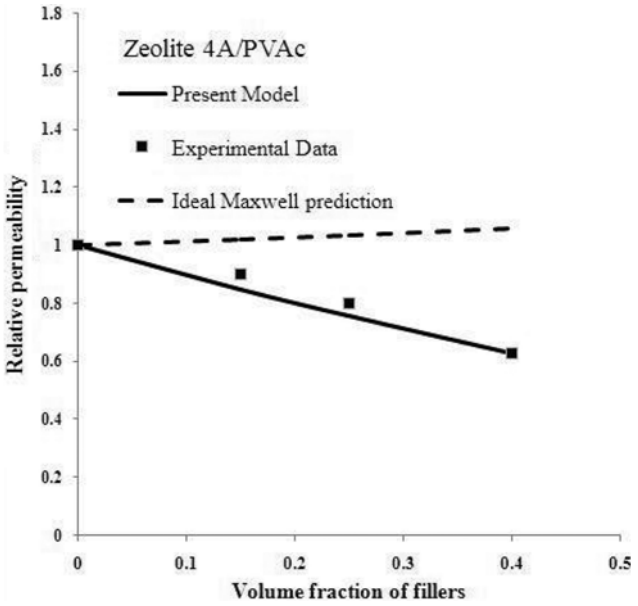

Fig. 10. Comparison between present model and ideal Maxwell model predictions with experimental relative permeability (set 2).

and the results are summarized in Table 11. In addition, the present prediction of O_2 relative permeability of MMM and ideal Maxwell model predictions are compared with experimental permeation data in Fig. 10.

From the minimum value of AARE, it can be concluded that the modified Maxwell permeation model with optimized parameters can satisfy the experimental data reasonably.

CONCLUSIONS

The morphology of different MMMs was successfully estimated using a comprehensive computational method. All possible MMM morphologies were taken into account here by using different experimental permeation data. Optimized morphological parameters for these different MMMs were calculated by considering minimum AARE%. Considering the obtained adjustable parameters, it can be concluded that pore blockage and polymer chain rigidification defects can simultaneously occur for C60/Matrimid MMMs. In case of ZIF-8/6FDA-DAM MMM, almost ideal morphology was predicted because all morphological parameters for this case were negligible. Also for Zeolite 4A/PVAc MMM, predictive morphological parameters indicated that rigidified interface layer morphology occurred.

REFERENCES

1. R. W. Baker, *Membrane Technology and Applications, 2nd Ed.*, 1, Wiley (2004).
2. H. Lin and B. D. Freeman, *J. Mol. Struct.*, **739**, 57 (2005).
3. E. McLeary, J. Jansen and F. Kapteijn, *Micropor. Mesopor. Mater.*, **90**, 198 (2006).
4. P. Pandey and R. Chauhan, *Prog. Polym. Sci.*, **26**, 853 (2001).
5. T.-S. Chung, L. Y. Jiang, Y. Li and S. Kulprathipanja, *Prog. Polym. Sci.*, **32**, 483 (2007).
6. Y. Li, W. B. Krantz and T. S. Chung, *AIChE J.*, **53**, 2470 (2007).
7. R. Mahajan and W. J. Koros, *Polym. Eng. Sci.*, **42**, 1420 (2002).
8. R. Mahajan, W. J. Koros and M. Thundyil, *Membr. Technol.*, **1999**, 6 (1999).
9. D. Q. Vu, W. J. Koros and S. J. Miller, *J. Membr. Sci.*, **211**, 335 (2003).
10. M. A. Semsarzadeh, B. Ghalei, M. Fardi, M. Esmaeeli and E. Vakili, *Korean J. Chem. Eng.*, **31**, 841 (2014).
11. M. Arjmandi, M. Pakizeh and O. Pirouzram, *Korean J. Chem. Eng.*, **32**, 1178 (2015).
12. R. Bouma, A. Checchetti, G. Chidichimo and E. Drioli, *J. Membr. Sci.*, **128**, 141 (1997).
13. R. Pal, *J. Colloid Interface Sci.*, **317**, 191 (2008).
14. T. T. Moore, R. Mahajan, D. Q. Vu and W. J. Koros, *AIChE J.*, **50**, 311 (2004).
15. J. C. Maxwell, Clarendon Press, Oxford (1881).
16. E. E. Gonzo, M. L. Parentis and J. C. Gottifredi, *J. Membr. Sci.*, **277**, 46 (2006).
17. G. Banhegyi, *Colloid. Polym. Sci.*, **264**, 1030 (1986).
18. T. Lewis and L. Nielsen, *J. Appl. Polym. Sci.*, **14**, 1449 (1970).
19. L. E. Nielsen, *J. Appl. Polym. Sci.*, **17**, 3819 (1973).
20. M. Aroon, A. Ismail, T. Matsuura and M. Montazer-Rahmati, *Sep. Purif. Technol.*, **75**, 229 (2010).
21. H. Vinh-Thang and S. Kaliaguine, *J. Membr. Sci.*, **452**, 271 (2014).
22. H. Vinh-Thang and S. Kaliaguine, *Chem. Rev.*, **113**, 4980 (2013).
23. S. A. Hashemifard, A. F. Ismail and T. Matsuura, *J. Membr. Sci.*, **347**, 53 (2010).
24. K. M. Gheimasi, T. Mohammadi and O. Bakhtiari, *J. Membr. Sci.*, **427**, 399 (2013).
25. J. A. Sheffel and M. Tsapatsis, *J. Membr. Sci.*, **295**, 50 (2007).
26. J. A. Sheffel and M. Tsapatsis, *J. Membr. Sci.*, **326**, 595 (2009).
27. T. Singh, D.-Y. Kang and S. Nair, *J. Membr. Sci.*, **448**, 160 (2013).
28. A.-C. Yang, C.-H. Liu and D.-Y Kang, *J. Membr. Sci.*, **495**, 269 (2015).
29. T.-S. Chung, S. S. Chan, R. Wang, Z. Lu and C. He, *J. Membr. Sci.*, **211**, 91 (2003).
30. C. Zhang, Y. Dai, J. R. Johnson, O. Karvan and W. J. Koros, *J. Membr. Sci.*, **389**, 34 (2012).
31. R. Mahajan and W. J. Koros, *Ind. Eng. Chem. Res.*, **39**, 2692 (2000).
32. S. Varanasi, O. Guskova, A. John and J.-U. Sommer, *J. Chem. Phys.*, **142**, 224308 (2015).
33. R. T. Adams, J. S. Lee, T.-H. Bae, J. K. Ward, J. Johnson, C. W. Jones, S. Nair and W. J. Koros, *J. Membr. Sci.*, **367**, 197 (2011).